ATRP Enhances Structural Correlations In Polymerization-Induced Phase Separation**

Journal Article

Author(s):
Sicher, Alba (ID); Whitfield, Richard (ID); Ilavsky, Jan; Saranathan, Vinodkumar; Anastasaki, Athina; Dufresne, Eric (ID)

Biomimetic Synthesis

ATRP Enhances Structural Correlations In Polymerization-Induced Phase Separation**

*Alba Sicher, Richard Whitfield, Jan Ilavsky, Vinodkumar Saranathan, Athina Anastasaki, and Eric R. Dufresne**

Abstract: Synthetic methods to control the structure of materials at sub-micron scales are typically based on the self-assembly of structural building blocks with precise size and morphology. On the other hand, many living systems can generate structure across a broad range of length scales in one step directly from macromolecules, using phase separation. Here, we introduce and control structure at the nano- and microscales through polymerization in the solid state, which has the unusual capability of both triggering and arresting phase separation. In particular, we show that atom transfer radical polymerization (ATRP) enables control of nucleation, growth, and stabilization of phase-separated poly-methylmethacrylate (PMMA) domains in a solid polystyrene (PS) matrix. ATRP yields durable nanostructures with low size dispersity and high degrees of structural correlations. Furthermore, we demonstrate that the length scale of these materials is controlled by the synthesis parameters.

Macromolecular materials often possess highly desirable properties that arise from their nano- and microstructure. For example, the filtration properties of membranes rely on their microscopic features,[1–4] and the structural color of colloidal coatings depends on the size of the particles they contain.[5–7] While synthetic nano- and micro-structured materials are commonly produced using self-assembly methods such as colloidal processing and block-copolymer assembly,[5–14] living systems generate structures in one step directly from macromolecules whose dimensions are much smaller than the characteristic scale of the final structure. For example, cells generate structures with pronounced order and low size dispersity through phase separation. Some examples include the photonic structures generating color in some bird feathers,[15–18] the topography of pollen's cell walls,[19] and the regular porosity of diatom frustules.[20–22] We have previously shown that polymerization-induced phase separation in the solid state can be used to make durable, nanostructured, and colorful materials.[23] This process starts with a glassy polymer matrix swollen and plasticized with a second monomer. When polymerization is triggered, the molecular weight of the new polymer increases and the matrix is depleted of monomer. The former decreases the solubility and motility of the new polymer. The latter re-vitrifies the matrix. When the new polymers reach their limiting molecular weight, they begin to phase separate. If the matrix revitrifies before the polymers have fully demixed, the system can arrest in a kinetically trapped state with microscopic domains. This process is inherently self-limiting, and can generate well-defined supramolecular structures in a continuous process.

Implemented with free-radical polymerization (FRP),[23] the phase-separated domains were localized to a layer near the surface of the material, and featured modest degrees of short-range translational order. These nanostructures gave the solid composite a blue or white color. We hypothesize that structural correlations were limited by the broad size distribution of the phase-separated domains, reflecting the broad range of initiation times and molecular weights typical of FRP,[24–26] represented schematically in Figure 1a–d.

Here, atom transfer radical polymerization (ATRP) was used to provide control over the nucleation and growth of phase-separated domains in the solid state. Controlled- (or living-) radical polymerization, and in particular ATRP, relies on fast initiation and yields narrow molecular weight distributions through suppression of termination events, as well as slow and sustained growth.[25, 27–32] In the solid state, we hypothesized that this would trigger the simultaneous nucleation of all the secondary-phase inclusions[33] (Figure 1f,g), yielding narrow size distributions. We obtained durable nanostructures with significantly improved size dispersity and structural correlations, and we could tune the

[*] A. Sicher, Prof. Dr. E. R. Dufresne
Laboratory for Soft and Living Materials, Department of Materials, ETH Zürich, Vladimir-Prelog-Weg 5/10, 8093 Zürich (Switzerland)
E-mail: eric.dufresne@mat.ethz.ch

Dr. R. Whitfield, Prof. Dr. A. Anastasaki
Laboratory of Polymeric Materials, Department of Materials, ETH Zürich, Vladimir-Prelog-Weg 5/10, 8093 Zürich (Switzerland)

Dr. J. Ilavsky
X-ray Science Division, Argonne National Laboratory, 9700 South Cass Avenue, Argonne, Illinois 60439 (United States)

Prof. Dr. V. Saranathan
Division of Sciences, School of Interwoven Arts and Sciences, Krea University, 5655, Central Expressway, Sri City, Andhra Pradesh 517646 (India)
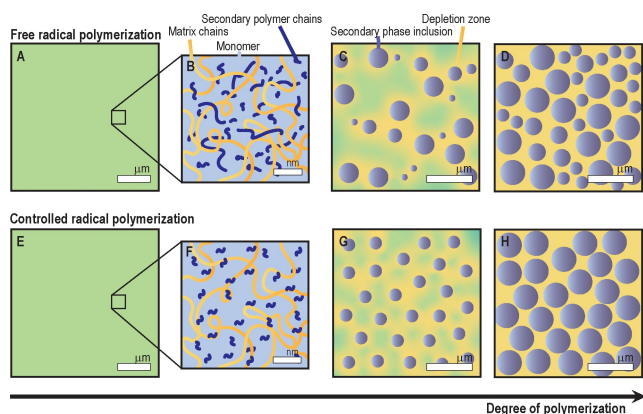
Figure 1. Comparison of FRP- and ATRP-induced phase separation. a), e) Uniform macroscopic conditions at the onset of the polymerization, before phase separation is triggered. A glassy matrix is swollen by a mixture of monomer and initiator. Green color indicates a mixture of blue and yellow components. b), f) Corresponding molecular views. We schematize the PS matrix in yellow, forming PMMA chains in blue, and MMA as a light-blue background pervading the system. c), g) Sche-ematics of the microscopic phase-separated inclusions. The PMMA inclusions are blue, and the area around them where the monomer is depleted is yellow. d), h) Expected difference in the final structure and dispersity following kinetic arrest.

Figure 2. Structure and correlations change during polymerization. a), b) STEM images of two ATRP samples polymerized for different times. For each sample we report the polymerization time, the fraction of PMMA (χ) and the degree of monomer conversion (η). c) Size distribution of the inclusions in panels (a), (b). On the x-axis: the apparent radius of particles on a 2D section of a 3D material. d), e) 2D distribution map calculated from the images in (a) and (b), respectively. The colorbar is reported at the bottom of each panel. The rings in the distribution maps are distorted as a consequence of the fabrication of the PS film through hot-pressing. f) Azimuthal average of plots (c), (d). Inset: the x-axis of the azimuthal average is normalized by the mode of each particle size distribution (r_0). In panels (c) and (f) the yellow curves correspond to the sample in (a), (d) and the green curves to the sample in (b), (e).

length scale in the material through control of the synthesis parameters.

We selected polystyrene (PS) and poly(methyl methacry-late) (PMMA), a model system for phase separation of binary polymer blends.[34–38] To prepare the samples, we first hot-pressed 1 mm thick polystyrene (PS) films to form the glassy matrices. We soaked them in mixtures of monomer (methyl methacrylate, MMA) and ethanol (EtOH) contain-ing all the necessary ATRP components. By diluting the reagents in ethanol, which does not partition into PS, we were able to tune their concentration in the matrix. The used amount of MMA in EtOH was varied between 30 % and 40 % wt, and the total amount of solution was large compared to the quantity of monomer able to partition in the PS film. We selected activators regenerated by electron transfer (ARGET) ATRP as our method,[39–41] as this yielded a homogeneous polymerization, where high con-versions, low dispersity and good control over molecular weight could be achieved with a bath ratio of [monomer]:[initiator]:[CuBr$_2$]:[ligand]:[Sn(2-ethylhexa-noate)] = 200:1:0.01:0.01:0.1.[42] The reaction was run at 70 °C. Full details of the experimental procedure and reaction design are described in the Supporting Information.

To understand how the structure develops, we used scanning transmission electron microscopy (STEM) and observed samples under indentical polymerization condi-tions at different time points. The results are visible in Figure 2. Panel a shows the center of a sample at 6 hours. At this time point, polymerization and phase separation are ongoing. Panel b shows the structure at 336 hours, after polymerization has completed and the structure has reached steady state. The size distributions of PMMA domains are shown in panel c. As polymerization and phase separation
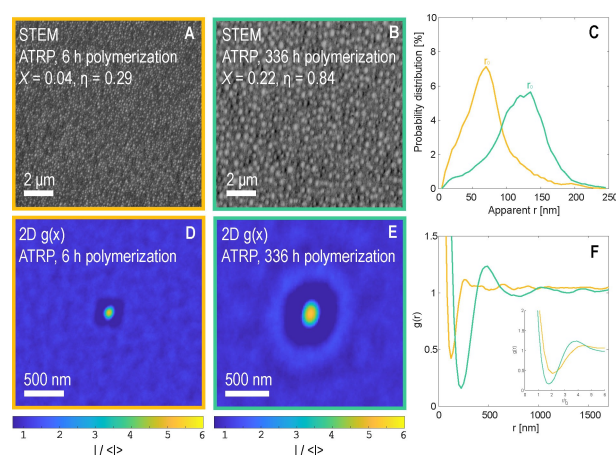
proceed, the radii of the inclusions increase from 70 nm to 130 nm. Note that phase-separated nanostructures are found throughout the bulk of the >1 mm-thick sample, not just near the surface, as previously found for FRP.[23]

To quantify structural correlations of the PMMA inclusions, we calculated a two dimensional distribution map, $g(\vec{x})$.[43,44] We computed $g(\vec{x})$ by averaging binarized areas of interest aligned with the center of each particle, and normalized with the average intensity in the binarized image, $\langle I \rangle$. The resulting image shows the average distribu-tion of particle density around a fixed particle (Figure 2d, e). At early polymerization stages, we observe a clear depletion zone around each particle (panel d). This makes sense, as particles grow by depleting polymer chains from their surroundings. As polymerization proceeds, structural corre-lations emerge. These correlations correspond to the bright ring around the center particle in panel e. This ring indicates a regular center-center particle distance between the domains. In other words, it quantifies a characteristic structural length scale in the system. The azimuthal average of the distribution map yields a radial distribution function, $g(r)$, shown in panel f. As the process proceeds, the peak of $g(r)$ moves to larger values of r. This indicates that the domains not only grow, but their spacing increases from 260 to 490 nm. Furthermore, the peak grows stronger as polymerization proceeds, with the peak value of $g(r)$ increasing from 1.1 to 1.2. This shows that domains become more evenly distributed. Together, these features indicate

that the particles retain some ability to rearrange within the matrix as they grow.

To gain some insight into the phase separation process, we sketch the path that the system follows during polymerization on a hypothetical phase diagram (Figure 3a). For simplicity, we ignore the continuous molecular-weight dependence of the solubility, and imagine that methyl methacrylate is either mononomeric (MMA) or polymeric. This schematic diagram has a few essential features. MMA and PS as well as MMA and PMMA are fully miscible, while PS and PMMA are immiscible. Below a critical monomer concentration, the material undergoes kinetic arrest (i.e. the matrix becomes glassy). The green path across the phase diagram shows the compositional shift of the two phases as the polymerization proceeds. After swelling, the system starts off on the MMA/PS axis. As polymerization starts, the system follows a contour of constant PS concentration. When the system reaches the boundary between the one- and two-phase regions of the phase diagram, it is saturated with polymer. With further polymerization, the system phase separates along the indicated tie-lines, creating PMMA- and PS-rich phases. Ultimately, phase separation stops when the PS-rich phase reaches the kinetic arrest line and vitrifies. In this picture, we expect the size of PMMA-rich domains to depend on the initial monomer loading. When relatively little monomer is loaded into the matrix, phase separation cannot proceed very far before the system vitrifies.

To quantify the effect of monomer loading on the microstructure, we used ultra-small-angle and small-angle X-ray scattering, (U)SAXS. Results for MMA-EtOH ratios from 30 to 40% are shown in Figure 3b. There, the scattering intensity, $I(q)$, is multiplied by the third power of the wavevector, q^3, to remove the characteristic large-q decay of collapsed polymer coils.[18,45,46] For each condition, multiple samples were prepared, measured, and plotted individually. As expected, we found smaller length scales for low monomer loading. Specifically, the position of the (U)SAXS peak shifted towards larger q values as we reduced the amount of MMA in EtOH. The characteristic wavevectors ranged from 0.0014 to 0.0055 Å^{-1}. In real space, these correspond to 450 and 110 nm, respectively. The obtained structures are stable over a period of at least 9 months (Figure S4).

As the scattering peaks shifted to larger q values, they also broadened. We make this trend more explicit by plotting the full width of the peak at 80% height (Δq) as a function of the peak position (q_0) in Figure 3c. As the monomer loading is varied, the relative width of the scattering peak is constant. $\Delta q/q_0 \approx 0.5$ for all the samples, as indicated by the linear fit, although samples made with the lowest monomer loading (30%) show larger sample-to-sample variability. The consistency of $\Delta q/q_0$ suggests that the process of phase-separation and arrest is scale-invariant over the explored parameter range.[16,18]

Next, we compare samples obtained with ATRP to those synthesized using FRP[23] and to some biological nano-structures thought to form through polymerization-induced phase separation.[16] Figure 4a shows the X-ray scattering intensities measured for a representative sphere-type bird feather (*Cotinga maynana*), and for the best FRP sample and ATRP sample. While the scattering peak of the *Cotinga* feather nanostructure remains unmatched, the ATRP sample shows comparable levels of structural correlations, with improved peak strength and narrowness compared to the FRP sample.

Figure 4b shows $\Delta q/q_0$ as a function of peak position, and compares different classes of synthetic and natural materials. Here, the peak width was measured directly from $I(q)$ instead of $q^3I(q)$, because different materials have different characteristic decays at large q. We find that $\Delta q/q_0$ is 0.74 and 0.42 for FRP and ATRP samples, respectively. The latter are comparable to channel-type biological samples, with the most strongly correlated ATRP sample ($\Delta q/q_0 \approx 0.3$) comparable to highly ordered sphere-type nanostructures.[16] Additionally, ATRP samples made with 30% MMA ($\Delta q/q_0 \approx 0.4$–0.5) have small enough inclusions to scatter blue light selectively, as shown in the inset.

In conclusion, we have designed a process that yields materials with spontaneously formed correlated structures at the sub-micron scale using phase separation. Compared to FRP, ATRP offers tuneable size, and stronger structural correlations. We expect that further reducing the nucleation time and molecular weight dispersity of polymeric chains will promote even lower particle size dispersity and higher
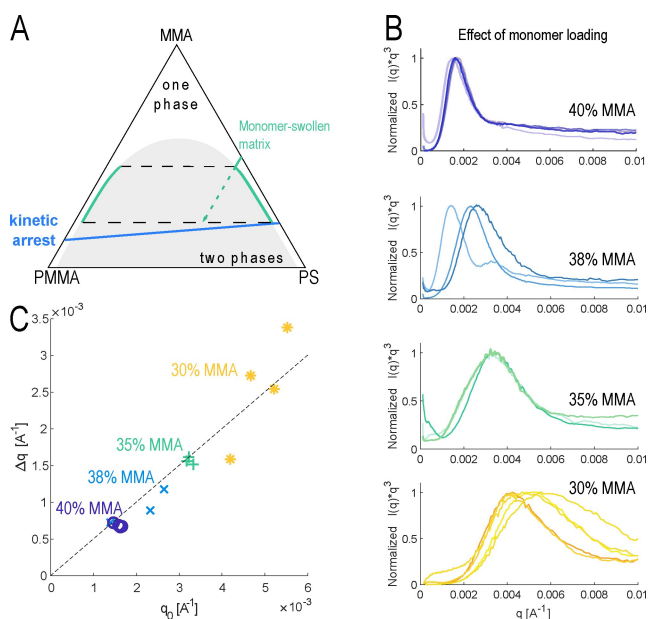

Figure 3. Effect of monomer loading on the structure. a) Hypothetical phase diagram. The two-phase region is colored in gray, the kinetic arrest line in blue, and the tie lines are dashed. The green path indicates the trajectory of a sample during polymerization. The dashed green line indicates the average composition, the solid green lines the composition of each phase. b) (U)SAXS profiles. Different lines on the same plot correspond to different samples synthesized in the same conditions at the same MMA-EtOH ratio. c) X-ray scattering peak width at 80% height (Δq) plotted as a function of the peak position (q_0) for each curve in (b). The linear fit highlights scale-invariant samples with the same degree of structural correlations (same $\Delta q/q_0$).
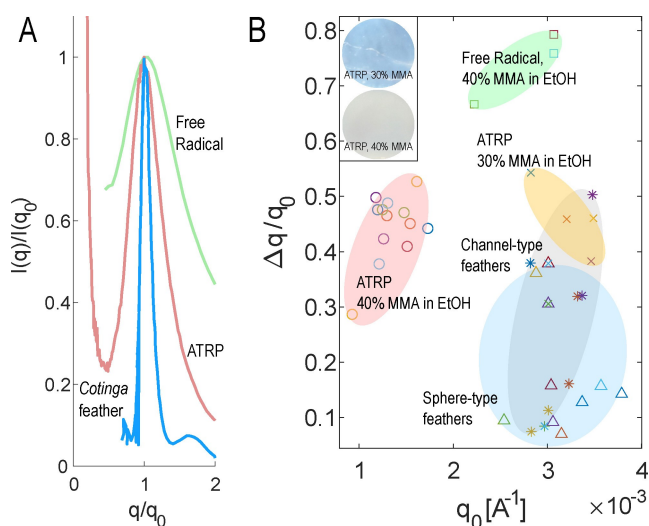
Figure 4. Structural correlations in phase-separated materials. a) Normalized (U)SAXS curves corresponding to the nanostructure in the feather barbs of *Cotinga maynana* (blue), and to two samples made with FRP (green) and ATRP (red), respectively. b) Diagram comparing the structural quality of PS-PMMA composites made with different strategies to biophotonic channel-(gray) and sphere-type nanostructures (blue) in bird feathers. Red: ATRP samples, 40% MMA, 60% EtOH. Yellow: ATRP samples, 30% MMA, 70% EtOH. Green: FRP samples. Inset: pictures of two ATRP samples made with 30 and 40% MMA; 8 mm diameter. Δq is the full width at 80% height. FRP data from ref. [23].

level of order in the system. Additionally, we anticipate that the adaptation of this approach to components with stronger tendency to phase separate, or different relative glass transitions, could unlock new phase-separated morphologies.[38] More broadly, controlled-radical polymerization could become a powerful tool to manipulate phase separation for the creation of durable nano-structured materials at scale.

Conflict of Interest

There are no conflicts of interest to declare.

Data Availability Statement

The data that support the findings of this study are available from the corresponding author upon reasonable request.

[1] I. Wienk, R. Boom, M. Beerlage, A. Bulte, C. Smolders, H. Strathmann, *J. Membr. Sci.* **1996**, *113*, 361.

[2] D.-M. Wang, J.-Y. Lai, *Curr. Opin. Chem. Eng.* **2013**, *2*, 229.

[3] M. F. Haase, H. Jeon, N. Hough, J. H. Kim, K. J. Stebe, D. Lee, *Nat. Commun.* **2017**, *8*, 1.

[4] C. Fernández-Rico, T. Sai, A. Sicher, R. W. Style, E. R. Dufresne, *JACS Au* **2022**, *2*, 66.

[5] J. D. Forster, H. Noh, S. F. Liew, V. Saranathan, C. F. Schreck, L. Yang, J.-G. Park, R. O. Prum, S. G. Mochrie, C. S. O'Hern, et al., *Adv. Mater.* **2010**, *22*, 2939.

[6] G. H. Lee, T. M. Choi, B. Kim, S. H. Han, J. M. Lee, S.-H. Kim, *ACS Nano* **2017**, *11*, 11350.

[7] G. Shang, M. Eich, A. Petrov, *APL Photonics* **2020**, *5*, 060901.

[8] K. Nagayama, *Colloids Surf. A* **1996**, *109*, 363.

[9] P. Jiang, J. Bertone, K. S. Hwang, V. Colvin, *Chem. Mater.* **1999**, *11*, 2132.

[10] K. Matsubara, M. Watanabe, Y. Takeoka, *Angew. Chem. Int. Ed.* **2007**, *46*, 1688; *Angew. Chem.* **2007**, *119*, 1718.

[11] A. C. Edrington, A. M. Urbas, P. DeRege, C. X. Chen, T. M. Swager, N. Hadjichristidis, M. Xenidou, L. J. Fetters, J. D. Joannopoulos, Y. Fink, et al., *Adv. Mater.* **2001**, *13*, 421.

[12] S. Valkama, H. Kosonen, J. Ruokolainen, T. Haatainen, M. Torkkeli, R. Serimaa, G. ten Brinke, O. Ikkala, *Nat. Mater.* **2004**, *3*, 872.

[13] C.-S. Wu, P.-Y. Tsai, T.-Y. Wang, E.-L. Lin, Y.-C. Huang, Y.-W. Chiang, *Anal. Chem.* **2018**, *90*, 4847.

[14] B. B. Patel, D. J. Walsh, D. H. Kim, J. Kwok, B. Lee, D. Guironnet, Y. Diao, *Sci. Adv.* **2020**, *6*, eaaz7202.

[15] E. R. Dufresne, H. Noh, V. Saranathan, S. G. Mochrie, H. Cao, R. O. Prum, *Soft Matter* **2009**, *5*, 1792.

[16] V. Saranathan, J. D. Forster, H. Noh, S.-F. Liew, S. G. Mochrie, H. Cao, E. R. Dufresne, R. O. Prum, *J. R. Soc. Interface* **2012**, *9*, 2563.

[17] R. O. Prum, *Bird coloration, Vol. 1*, Harvard University Press, Boston, **2006**, p. 295.

[18] V. Saranathan, S. Narayanan, A. Sandy, E. R. Dufresne, R. O. Prum, *Proc. Natl. Acad. Sci. USA* **2021**, *118*, e2101357118.

[19] A. Radja, E. M. Horsley, M. O. Lavrentovich, A. M. Sweeney, *Cell* **2019**, *176*, 856.

[20] M. Sumper, *Science* **2002**, *295*, 2430.

[21] L. Lenoci, P. J. Camp, *Langmuir* **2008**, *24*, 217.

[22] M. Feofilova, S. Schüepp, R. Schmid, F. Hacker, H. T. Spanke, N. Bain, K. E. Jensen, E. R. Dufresne, *Proc. Natl. Acad. Sci. USA* **2022**, *119*, e2201014119.

[23] A. Sicher, R. Ganz, A. Menzel, D. Messmer, G. Panzarasa, M. Feofilova, R. O. Prum, R. W. Style, V. Saranathan, R. M. Rossi, et al., *Soft Matter* **2021**, *17*, 5772.

[24] C. S. Sheppard, V. R. Kamath, *Polym. Eng. Sci.* **1979**, *19*, 597.

[25] K. Matyjaszewski, *Macromolecules* **2012**, *45*, 4015.

[26] H. S. Bisht, A. K. Chatterjee, *J. Macromol. Sci. C* **2001**, *41*, 139.

[27] K. Matyjaszewski, *Adv. Mater.* **2018**, *30*, 1706441.

[28] A. Goto, T. Fukuda, *Prog. Polym. Sci.* **2004**, *29*, 329.

[29] K. Matyjaszewski, J. Xia, *Chem. Rev.* **2001**, *101*, 2921.

[30] M. R. Hill, R. N. Carmean, B. S. Sumerlin, *Macromolecules* **2015**, *48*, 5459.

[31] X. Pan, M. A. Tasdelen, J. Laun, T. Junkers, Y. Yagci, K. Matyjaszewski, *Prog. Polym. Sci.* **2016**, *62*, 73.

[32] B. M. Rosen, V. Percec, *Chem. Rev.* **2009**, *109*, 5069.

[33] P. J. Flory, *J. Chem. Phys.* **1942**, *10*, 51.

[34] C. Ton-That, A. Shard, R. Daley, R. Bradley, *Macromolecules* **2000**, *33*, 8453.

[35] D. C. Sundberg, Y. G. Durant, *Polym. React. Eng.* **2003**, *11*, 379.

[36] C. Dekeyser, S. Biltresse, J. Marchand-Brynaert, P. Rouxhet, C. C. Dupont-Gillain, *Polymer* **2004**, *45*, 2211.

[37] Y. Zhao, E. Sivaniah, T. Hashimoto, *Macromolecules* **2008**, *41*, 9948.

[38] P. Zhang, D. C. Sundberg, J. G. Tsavalas, *Ind. Eng. Chem. Res.* **2019**, *58*, 21118.

[39] Y. Kwak, A. J. Magenau, K. Matyjaszewski, *Macromolecules* **2011**, *44*, 811.

[40] A. Simakova, S. E. Averick, D. Konkolewicz, K. Matyjaszewski, *Macromolecules* **2012**, *45*, 6371.

[41] R. Whitfield, K. Parkatzidis, K. G. Bradford, N. P. Truong, D. Konkolewicz, A. Anastasaki, *Macromolecules* **2021**, *54*, 3075.

[42] N. Chan, M. F. Cunningham, R. A. Hutchinson, *Macromol. Chem. Phys.* **2008**, *209*, 1797.

[43] N. Mac Fhionnlaoich, R. Qi, S. Guldin, *Langmuir* **2019**, *35*, 16605.

[44] T. J. Böddeker, K. A. Rosowski, D. Berchtold, L. Emmanouilidis, Y. Han, F. H. Allain, R. W. Style, L. Pelkmans, E. R. Dufresne, *Nat. Phys.* **2022**, *18*, 571.

[45] O. Glatter, O. Kratky, H. Kratky, *Small angle X-ray scattering*, Academic Press, New York, **1982**.

[46] M. Pérez Méndez, D. Rodríguez Martínez, J. Fayos, *Int. J. Adv. Eng. Technol. Manage. Appl. Sci.* **2016**, *3*, 27–41.